

## Observation of Crystallization of Vapor-deposited TPD Films by AFM and FFM

Eun-mi HAN, Lee-mi DO, Yasuro NIIDOME, and Masamichi FUJIHIRA\*

Department of Biomolecular Engineering, Tokyo Institute of Technology, Nagatsuta, Midori-ku, Yokohama 227

The morphological change of vapor-deposited TPD (N,N'-diphenyl-N,N'-bis-(3-methylphenyl)-[1,1'-biphenyl]-4,4'-diamine) films, used as the hole transport layer of organic electroluminescent (EL) devices, on a glass plate was observed by atomic force microscopy (AFM) and friction force microscopy (FFM) in an ambient atmosphere. The TPD film was flat and amorphous as deposited, but was crystallized partially about a week later. By friction force loop measurement, we found that the bare glass surface was revealed between the crystals and between the amorphous film and the crystal due to mass transport for crystallization of TPD from the amorphous film.

Electroluminescent (EL) devices based on organic thin layers have attracted much attention because of their possible application as large-area light-emitting displays. Organic EL devices have the advantage over inorganic ones of being driven by low dc voltage, highly luminescent, and multicolor emissive by their molecular design. But it is still far from practical use because of the lack of running stability and durability. Most of the researchers have concentrated their attention on long-term stability of organic EL devices. There have been, however, few report on the origin of degradation of organic EL devices.<sup>1-4)</sup> As one of the origin of the degradation of organic EL devices, it is assumed that the failure is attributed to the degradation of both hole and electron injecting contacts.<sup>2)</sup> In order to increase EL efficiency and stability, many researchers took the focus upon further improvement in an organic material with the necessary EL properties. Although the crystallization of a TPD (i.e. N,N'-diphenyl-N,N'-bis-(3-methylphenyl)-[1,1'-biphenyl]-4,4'-diamine) layer under continuous operation was reported,<sup>3)</sup> until now TPD has been used most widely as the hole transport layer in organic EL devices due to high carrier mobility and amorphous film-forming ability.<sup>5)</sup>

In this letter, to explain the mechanism of degradation of organic EL devices, we directly observed the morphological change of the vapor-deposited TPD films under an ambient atmosphere by atomic force microscopy (AFM) and friction force microscopy (FFM).

The AFM<sup>6,7)</sup> has been used to characterize the surfaces of organic materials on the atomic scale.<sup>8)</sup> The FFM, a modified AFM,<sup>9)</sup> can be a powerful tool in characterizing heterogeneous material surfaces by merely measuring the deflection of the cantilever in response to lateral force.<sup>10-14)</sup> The FFM used in this study detects normal and lateral forces simultaneously by using a laser beam deflection technique.<sup>7,15,16)</sup> The measurements of AFM and FFM were carried out with a SEIKO SPA-300 unit controlled with a SPI-3700 controller. Olympus microfabricated rectangular Si<sub>3</sub>N<sub>4</sub> cantilevers of 200  $\mu$ m-long with normal and torsion spring constants of 0.09 and 315.40 Nm<sup>-1</sup> were used. All observations were carried out under an ambient atmosphere. TPD was deposited on optical glass substrates by vapor deposition under a vacuum of about 10<sup>-6</sup> Torr. The deposition rate

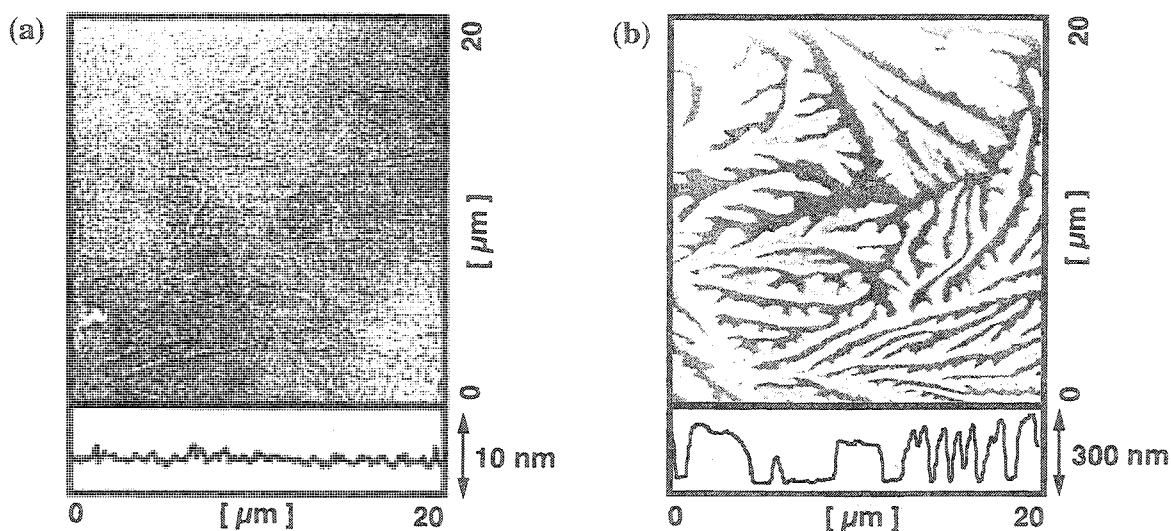


Fig. 1. AFM images (upper) and cross-sections (lower) of the morphology change of a TPD film under an ambient atmosphere; (a) as-deposited TPD film, (b) crystallized TPD film. The scan range is  $20 \times 20 \mu\text{m}^2$ . Cross-sections taken from the center line on the AFM images (upper). The height of cross-sections are (a) 10 nm and (b) 300 nm, respectively.

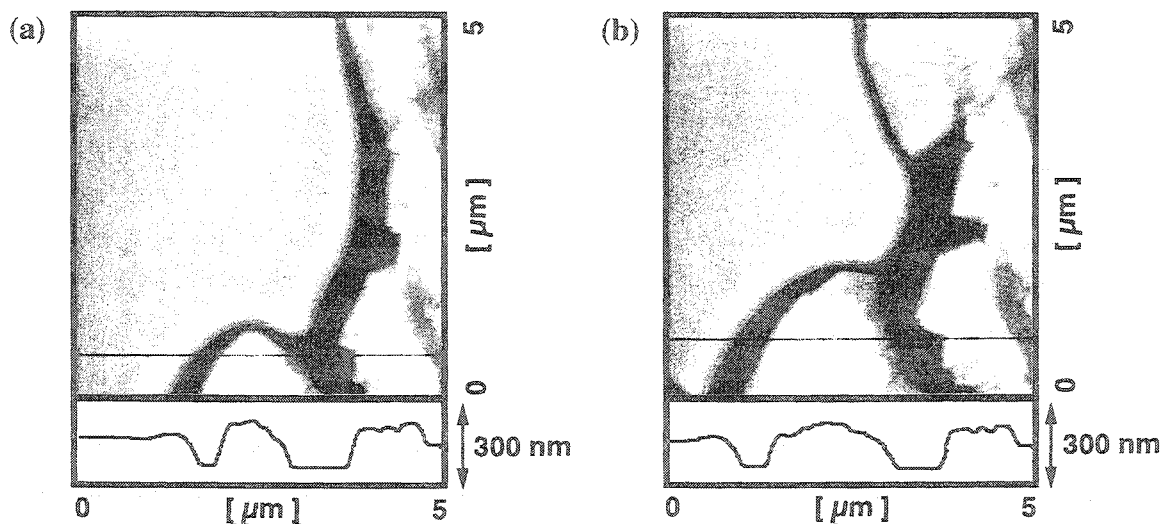


Fig. 2. The morphological change on a TPD film for an hour under an ambient atmosphere; (a) first scan, (b) second scan after 1 h of scan (a). Brightness connotes height. The scan range is  $5 \times 5 \mu\text{m}^2$ .

of TPD was about  $2 - 3 \text{ \AA s}^{-1}$ .

The change of AFM images (upper) and their cross-sections (lower) of vapor-deposited TPD film are shown in Fig. 1. All AFM images are the size of  $20 \times 20 \mu\text{m}^2$ . White areas correspond to higher parts in the AFM topographic images (upper). The as-deposited TPD film (Fig. 1 (a)) exhibited an entirely amorphous and flat surface with average roughness,  $R_a$ , of ca. 0.6 nm. About a week later, however, the AFM image of TPD film became distinctive due to partial crystallization as described later. Figure 1(b) represents a completely crystallized TPD film after 3 months later. Along with the crystallization of TPD film, it is clearly seen from the cross-section of Fig. 1(b) that the valleys were also created between crystals. The valley formation was necessary, because the heights of the crystals were much higher than that of the as-deposited TPD film.

We also observed the growth of crystals on the same position by observing two successive AFM images

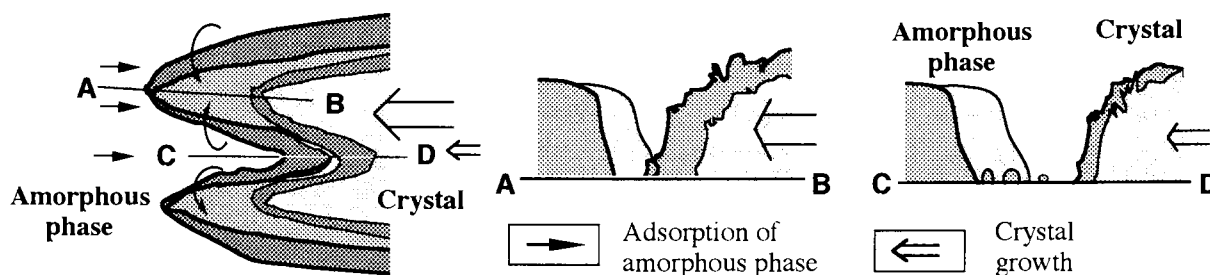


Fig. 3. Schematic illustration for the crystal growth of a TPD film. Top view (left) and side view (right).

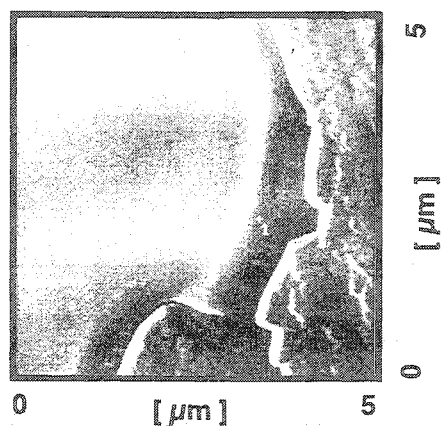


Fig. 4. Friction force map on the same area of the partially crystallized TPD film as the topographic image in Fig. 2(a). Brightness connotes higher friction. The scan range is  $5 \times 5 \mu\text{m}^2$ .

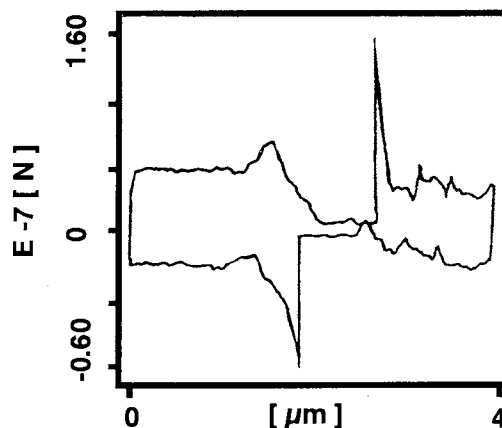


Fig. 5. Friction force loop taken along a line centered by the cross mark in the friction map of Fig. 4.

after an interval of 1 h. As shown in Fig. 2, the crystal growth is clearly seen with AFM in an ambient atmosphere. From the cross-sections of the TPD film of Fig. 2, we found the depth of lowest valleys from the plateau of the amorphous film is nearly equal to the thickness of the as-deposited TPD film itself. It indicates that the substrate surface was revealed by the crystallization.

We illustrate schematically the process of the morphological change of the TPD film due to the crystallization in Fig. 3. The white arrows represent the direction and magnitude of the crystal growth. The mass transport from the amorphous phase to the front of the crystal growth is extremely high where the velocity of the crystal growth toward the amorphous phase is much higher than those of the neighboring sites. The fast growing crystal front on the line between A and B adsorbs TPD molecules from the amorphous bank surrounding the growing front. In contrast, TPD molecules from the amorphous bank on the line between C and D are transported not only toward the crystal front in the opposite bank of the valley but also toward the neighboring growing fronts. Therefore, the much faster depletion of the amorphous phase surrounding the valleys on the line between C and D resulted in the increase in the width of the valley on the line with crystal growth.

To distinguish between the surfaces of the TPD amorphous and crystal films and the exposed substrate surface at the bottom of the valleys, we observed the corresponding FFM image which allows to differentiate the chemical inhomogeneities of the films by difference in the frictions. Figure 4 shows the friction map of a partially crystallized TPD film which was observed simultaneously with the AFM topography of Fig. 2(a). White areas correspond to the region with high lateral forces. In the friction image, no remarkable difference

in frictions is measurable on surfaces of the crystalline and the amorphous films, while a much lower lateral force was observed at the bottom of the valleys as shown in Fig. 4. The result suggests that the area with the low friction is not TPD covered glass but corresponds to the bare substrate.

For the quantitative measurement of the friction forces on the heterogeneous surface, we recorded the friction forces during the forward and backward scans on the same line of the film surface, which is known as a *friction force loop*,<sup>11)</sup> as shown in Fig. 5. The difference between upper and lower curves divided by two yields the friction force. The friction force loop was taken along a line centered by the cross mark in the friction map of Fig. 4. The applied normal force was ca. 12 nN. The lowest friction force was about 5 nN and was observed on the exposed substrate, while the highest friction force on the amorphous phase and the medium friction force on the crystal were about 30 and 24 nN, respectively. These values were obtained from the friction force loop. The friction of the amorphous phases is somewhat higher than that of the crystal. The result can be explained by the ease of deformation of the softer amorphous surface and thus the larger area of contact between the tip and the sample surface.

From the above surface observation of the vapor-deposited TPD film with time by means of AFM and FFM, we found that the entirely amorphous and flat film of the as deposited one was partially crystallized in an ambient atmosphere. With an increase in the crystallization of TPD, the deep valleys appeared in the film and the bare substrate surface was exposed. FFM was successfully used for chemical differentiation between the TPD film covered and the exposed glass surfaces.

In conclusion, the process of crystal growth of the vapor-deposited TPD amorphous film on the glass substrate was successfully observed *in situ* by AFM. The FFM can be used to differentiate the surfaces of amorphous and crystalline TPD films from the exposed substrate surface. From the friction force loop measurements, it is evident that the bare substrate was exposed with crystallization of the TPD film. In the practical operation of organic EL cells, detachment of a TPD hole transport layer from an ITO base electrode and thus the decrease of the effective contact area due to the crystallization of TPD may decrease the EL efficiency. In addition, the crystallization of TPD film layer can be accelerated by the Joule heat produced in the organic EL cells.

## References

- 1) P. S. Vincett, W. A. Barlow, R. A. Hann, and G. G. Roberts, *Thin Solid Films*, **94**, 171 (1982).
- 2) C. W. Tang and S. A. VanSlyke, *Appl. Phys. Lett.*, **51**, 913 (1987).
- 3) C. Adachi, T. Tsutsui, and S. Saito, *Appl. Phys. Lett.*, **56**, 799 (1990).
- 4) Y. Hamada, C. Adachi, T. Tsutsui, and S. Saito, *Jpn. J. Appl. Phys.*, **31**, 1812 (1992).
- 5) M. Abkowitz and D. M. Pai, *Philos. Mag. B*, **53**, 193 (1986).
- 6) G. Binnig, C. F. Quate, and Ch. Gerber, *Phys. Rev. Lett.*, **56**, 930 (1986).
- 7) G. Meyer and N. M. Amer, *Appl. Phys. Lett.*, **56**, 2100 (1990).
- 8) J. Frommer, *Angew. Chem., Int. Ed. Engl.*, **31**, 1298 (1992).
- 9) C. M. Mate, G. M. McClelland, R. Erlandsson, and S. Chiang, *Phys. Rev. Lett.*, **59**, 1942 (1987).
- 10) R. M. Overney, E. Meyer, J. Frommer, D. Brodbeck, R. Lüthi, L. Howald, H.-J. Güntherodt, M. Fujihira, H. Takano, and Y. Gotoh, *Nature*, **359**, 133 (1992).
- 11) E. Meyer, R. Overney, R. Lüthi, D. Brodbeck, L. Howald, J. Frommer, H.-J. Güntherodt, O. Wolter, M. Fujihira, H. Takano, and Y. Gotoh, *Thin Solid Films*, **220**, 132 (1992).
- 12) E. Meyer, R. Overney, D. Brodbeck, L. Howald, R. Lüthi, J. Frommer, and H.-J. Güntherodt, *Phys. Rev. Lett.*, **69**, 1777 (1992).
- 13) M. Fujihira and H. Takano, *Thin Solid Films*, in press.
- 14) M. Fujihira and Y. Morita, *J. Vac. Sci. Tech. B*, in press.
- 15) O. Marti, J. Colchero, and J. Mlynek, *Nanotechnology*, **1**, 141 (1990).
- 16) G. Meyer and N. M. Amer, *Appl. Phys. Lett.*, **57**, 2089 (1990).

( Received March 11, 1994 )